Multifrequency and Multiload MCR-WPT System Using Hybrid Modulation Waves SPWM Control Method

Chenyang Xia, *Member, IEEE*, Nan Wei, Hongtai Zhang, Shuze Zhao, Zhuang Li, and Zhijuan Liao

***Abstract*—To satisfy independent and controllable power supply requirements for loads with different frequencies and power levels, a multifrequency and multiload (MFML) magnetic coupling resonant wireless power transfer (MCR-WPT) system using hybrid modulation waves sinusoidal pulsewidth modulation (HMW-SPWM) control method is proposed in this article. Based on SPWM, loading a hybrid modulation wave formed by superimposing multifrequency modulation waves to drive the inverter, so the multifrequency hybrid current on the primary side can be obtained. According to the principle of mutual inductance coupling, inductive power with different frequencies is obtained and then separated by multiresonant networks on the secondary side for loads with different frequencies. First, the structure and working principle of a MFML MCR-WPT system controlled by HMW-SPWM are introduced. Then, taking a dual-frequency and dual-load MCR-WPT system as an example, the system is mathematically modeled. Besides, parameters design criteria for reducing interfrequency interference is studied. After that, load characteristics and power factor are analyzed to select appropriate parameters. Furthermore, dynamic characteristics are analyzed. Finally, theoretical results are validated by experiments. The experimental results show that the MFML MCR-WPT system controlled by HMW-SPWM realizes independent and controllable wireless power supply for loads with different frequencies and power levels.**

***Index Terms*—Hybrid modulation wave, multifrequency, multiload, SPWM control, wireless power transfer (WPT).**

I. Introduction

MAGNETIC coupling resonant wireless power transfer (MCR-WPT) is a new technology which realizes the wireless and flexible power transfer [1]–[3]. It is regarded as an important way to achieve clean, flexible, and efficient use of energy, which has been widely used in electric vehicles [4], aerospace and navigation [5], smart grid [6], new energy power generation [7], medical instruments [8], portable communication equipment [9], etc.

In recent years, with the development, application, and popularization of MCR-WPT technology, the research and application have gradually expanded from the initial single-load wireless power supply mode to the multiload synchronous wireless power supply mode. For a multiload MCR-WPT system, a lot of research has been done in different areas. According to whether the resonance frequency of each load is the same or not, the multiload MCR-WPT system can be classified into two types of working modes, one is the multiload MCR-WPT system with a same frequency, and the other one is the multifrequency and multiload (MFML) MCR-WPT system.

1) For the multiload MCR-WPT system with a same frequency, since the working frequency of each load is the same, it is only necessary to add a power conversion device to each load to realize independent power control [10]–[16]. However, although this type of multiload MCR-WPT system has been widely used, only the loads working at the single frequency can be powered since the natural frequencies of the primary and secondary circuits are consistent, which is not suitable for the loads working at other frequencies.
2) For the MFML MCR-WPT system, the different design targets, application environments, the working frequencies of various wireless charging products are not same, which severely reduces the products compatibility and increases system design and operating cost. To realize independent and controllable wireless power supply for the loads with different frequencies, the commonly used methods include multiprimary inverters parallel operation mode [17]–[19], multiresonant frequencies operation control mode [20], and power supply mode of different time periods [21]. In [17], a multifrequency circuit topology based on multiple inverters is proposed to achieve the multifrequency excitation of the system. On the basis of achieving high system efficiency, a new idea for power distribution of multiload is introduced. In [18], two different inverters are utilized to design a WPT transmitter that can work at 200 kHz and 6.78 MHz simultaneously, so as to supply power to two receivers of different frequency standards. Zhang *et al.* [19] present a circuit with the multitransmitting and multireceiving structure, and a multiphase multifrequency system with multiple

Manuscript received November 18, 2020; revised January 19, 2021 and March 18, 2021; accepted April 28, 2021. Date of publication May 14, 2021; date of current version July 30, 2021. This work was supported in part by the National Natural Science Foundation of China under Grant 51777210, and in part by the Six Talent Peaks Project in Jiangsu Province under Grant XNYQC-012. Recommended for publication by Associate Editor J. Acero. *(Corresponding author: Chenyang Xia.)*

The authors are with the Jiangsu Province Laboratory of Mining Electric and Automation, China University of Mining and Technology, Xuzhou 221008, China (e-mail: bluesky198210@163.com; wn18852279016@163.com; 3465281940@qq.com; 1171954566@qq.com; 772004992@qq.com; zjliao@cumt.edu.cn).

Color versions of one or more figures in this article are available at https://doi.org/10.1109/TPEL.2021.3079229.

Digital Object Identifier 10.1109/TPEL.2021.3079229

loads is proposed to realize targeted power distribution among loads. In [20], the multitransmitting and multireceiving structure is also adopted, based on multifrequency programmed pulsewidth modulation, each pair of transmitting and receiving coils are adapted to the designed working frequency, and the power transfer of the target frequency is realized, respectively. In [21], according to the maximum quality factor Q of the coils and the minimum frequency interference, three optimal working frequencies are determined. Power supply of different frequencies provides power to three loads in time intervals to achieve load isolation and power distribution.

Nevertheless, in order to meet the independent and controllable wireless power supply requirements for the MFML MCR-WPT system, there are several deficiencies in the methods mentioned above as follows.

1) Multiple inverters or multiple transmitting coils at the transmitting end will seriously affect the power transfer capacity and efficiency of the system and increase the cost of system.
2) Multifrequency power transfer is realized based on the parallel work of multiple inverters. However, due to the limited number of resonant frequencies, and for a specific system, its multiple resonant frequencies are fixed, so only the loads working at the same frequencies can gain power.
3) The system supplies power to loads with different frequencies in time intervals, but it is impossible to supply power to multiload with different working frequencies at the same time.

Therefore, the existing MFML wireless power supply methods cannot effectively meet the MFML wireless power supply requirements of MCR-WPT system.

In order to overcome the disadvantages mentioned above and meet the compatibility of different frequency loads, such as intelligent terminals charging [9], double-sided wireless charging [22], etc., an MFML MCR-WPT system using hybrid modulation waves sinusoidal pulsewidth modulation (HMW-SPWM) control method is proposed in this article, which can quickly and accurately realize multifrequency power output and meet the wireless power supply requirements of different power levels from several watts to kilowatts. Under the premise of ensuring the independent and reliable power transfer of different frequencies, the corresponding modulation wave signal frequencies are adjusted to the resonant frequencies of the loads on the secondary side, and the corresponding modulation wave signal amplitudes are adjusted to meet the power supply requirements for different loads, thereby achieving MFML independent power transfer and efficient power transfer control.

This article is organized as follows. The structure and working principle of the MFML MCR-WPT system controlled by HMW-SPWM are introduced in Section II. In Section III, system modeling is carried out, and the mathematical expressions of current response, output power, and efficiency of the loads with different frequencies are derived. The system parameters design criteria is discussed to reduce the interference of different frequencies in Section IV. The load characteristic and power factor of the system are analyzed to select the appropriate system parameters and optimize the output power of receiving circuits in Section V. In Section VI, the MFML MCR-WPT system using HMW-SPWM control method is verified by the simulation and experiment. Finally, Section VII concludes the article.

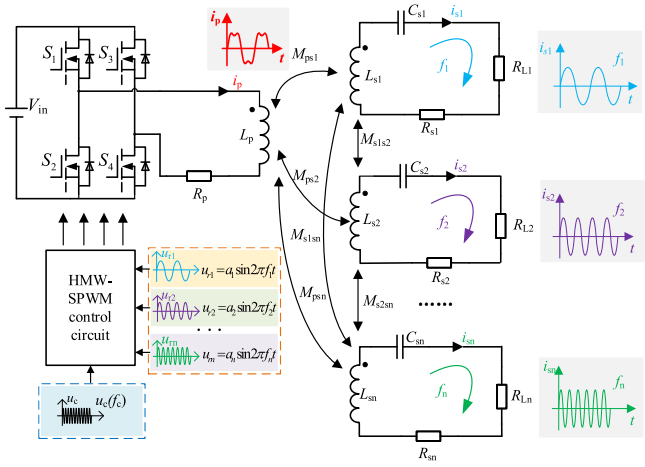

Fig. 1. Structure diagram of the multifrequency and multiload MCR-WPT system using HMW-SPWM control method.

II. Structure and Working Principle of Multifrequency and Multiload MCR-WPT System Using HMW-SPWM Control Method

Fig. 1 shows the structure diagram of the MFML MCR-WPT system using HMW-SPWM control method.

In Fig. 1, the MFML MCR-WPT system using HMW-SPWM control method contains a dc source, a high-frequency inverter, a primary power transmitting coil, an MFML power receiving device, and an HMW-SPWM control circuit. The primary side of the system adopts a zero compensation strategy, that is, there is only a single transmitting coil L_p. The MFML power receiving device on the secondary side includes n power receiving coils and n resonance compensation capacitors, which constitute n resonance compensation circuits, respectively. The natural resonant frequencies of the secondary side pick-up circuits are $f_1, f_2, \ldots, f_n$, respectively. Among them, L_{s1}, C_{s1} constitute a frequency f_1 selection network, L_{s2}, C_{s2} constitute a frequency f_2 selection network, L_{sn}, C_{sn} constitute a frequency f_n selection network, and the output ends of different resonant networks are, respectively, connected to the loads R_{L1}, R_{L2}, …, R_{Ln}. M_{psi}, and M_{sisj} ($i = 1, 2, \ldots, n, j = 12, \ldots, n, i < j$) are the mutual inductances between the transmitter and receivers and the cross mutual inductances between the secondary coils. R_P, R_{s1}, R_{s2}, …, R_{sn} are the equivalent series resistances.

The relationship between the parameters of the MFML power receiving device on the secondary side is

$$\begin{cases} (2\pi f_1)^2 L_{s1} C_{s1} = 1 \ \text{Power receiving circuit 1} \\ (2\pi f_2)^2 L_{s2} C_{s2} = 1 \ \text{Power receiving circuit 2} \\ \cdots\cdots \\ (2\pi f_n)^2 L_{sn} C_{sn} = 1 \ \text{Power receiving circuit } n. \end{cases} \tag{1}$$

The carrier wave of the HMW-SPWM control circuit is a triangular wave u_c, and the modulation wave adopts a hybrid

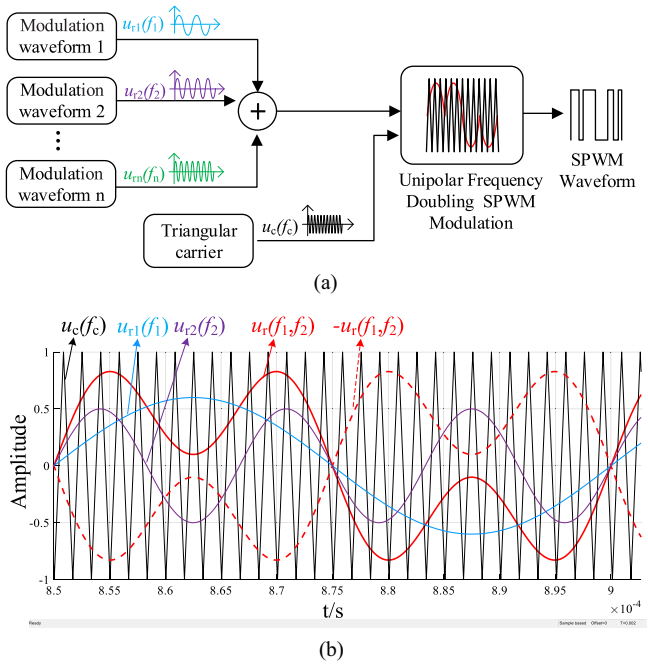

Fig. 2. Schematic diagram of the unipolar frequency doubling HMW-SPWM control circuit. (a) HMW-SPWM principle. (b) Comparison of carrier and modulation wave.

modulation wave u_r superimposed by multiple sine waves with adjustable amplitude and frequency. The hybrid modulation wave signal u_r is

$$\begin{aligned} u_r &= u_{r1} + u_{r2} + \ldots + u_{rn} \\ &= a_1 \sin 2\pi f_1 t + a_2 \sin 2\pi f_2 t + \ldots + a_n \sin 2\pi f_n t \end{aligned} \tag{2}$$

where $a_1, a_2, \ldots, a_n$ are the amplitudes of the modulation wave signals and $a_1, a_2 \ldots a_n \in (0, 1)$.

In order to avoid overmodulation and remain within the valid PWM working range, the amplitude of the hybrid modulation wave does not exceed the carrier amplitude. In addition, the switching frequency of the inverter is consistent with the carrier frequency f_c, and the frequency f_r of the modulation wave is equal to the ratio of the carrier frequency f_c to the carrier ratio N ($f_r = f_c/N$). According to the transmission frequencies $f_1, f_2 \ldots$, the carrier frequency is set to be consistent with the least common multiple of transmission frequencies. Thus, the carrier ratio N is guaranteed to be an integer to avoid additional harmonic interference. According to the requirements of the switching frequency of the inverter and the carrier ratio, the upper limit of the frequency of the modulation wave can be determined.

To reduce the output harmonics, the control circuit adopts the unipolar frequency doubling SPWM control, and the schematic diagram of the HMW-SPWM control circuit is shown in Fig. 2.

Based on the structure diagram of the MFML MCR-WPT system using HMW-SPWM control method in Fig. 1 and the schematic diagram of the HMW-SPWM control circuit in Fig. 2, the working principles of the MFML MCR-WPT system controlled by HMW-SPWM are as follows.

1) According to the natural resonant frequencies $f_1, f_2, \ldots, f_n$ of the secondary circuits where the different loads $R_{L1}, R_{L2}, \ldots, R_{Ln}$ are located, the modulation wave signals with the corresponding frequencies $f_1, f_2, \ldots, f_n$ are set. The amplitudes $a_1, a_2, \ldots, a_n$ of the modulation waves with different frequencies are designed according to power requirements of different loads.
2) In order to reduce the switching loss of inverter and avoid waveform distortion, the unipolar frequency doubling SPWM control [23], [24] is adopted in this article, that is, two modulation waves with the same amplitudes and opposite polarities are modulated with the carrier to generate drive signals.

The inverter output harmonics are concentrated in the high-frequency range of $2 \times m \times f_c$ ($m = 1, 2, 3, \ldots$), where f_c is the carrier frequency. The PWM waves contain very few low-order harmonics, and the harmonics are mainly concentrated near twice and more carrier frequency. The effect of these high-order harmonics is small, which does not cause strong EMI/EMC problems to the receivers.

The basic modulation method: the power modulation waves with different frequencies $f_1, f_2, \ldots, f_n$ and different amplitudes $a_1, a_2, \ldots, a_n$ are summed to obtain a hybrid modulation wave signal u_r and the inverse is $-u_r$. The signals modulated by the hybrid modulation wave u_r and the triangular carrier u_c are used as the driving signals of the front bridge arm, and the signals modulated by the hybrid modulation wave $-u_r$ and the triangular carrier u_c are used as the driving signals of the rear bridge arm. Thus, the high-frequency hybrid pulse waves containing different frequencies are generated after the high-frequency inverter.

1) Based on the electromagnetic induction coupling principle, each load obtains power of corresponding frequencies through resonant networks on the secondary side, so as to realize wireless power transfer to the loads with different frequencies in the system.
2) According to different frequencies and power requirements, the frequency and amplitude of each modulation wave of the HMW-SPWM controller are adjusted, that is, the carrier ratio and modulation degree of each modulation wave of the HMW-SPWM controller are correspondingly altered, and then directional power transfer and independent power control can be realized in the MFML MCR-WPT system.

III. Modeling of the Multifrequency and Multiload MCR-WPT System Using HMW-SPWM Control Method

A. System Modeling

In order to simplify the analysis, the structure diagram of a dual-frequency and dual-load MCR-WPT system using HMW-SPWM control method shown in Fig. 3 is studied, and its analysis method can be extended to other MFML MCR-WPT systems controlled by HMW-SPWM.

According to the frequency requirements of two loads, the hybrid modulation wave of the HMW-SPWM controller is set as

$$u_r = u_{r1} + u_{r2} = a_1 \sin 2\pi f_1 t + a_2 \sin 2\pi f_2 t. \tag{3}$$

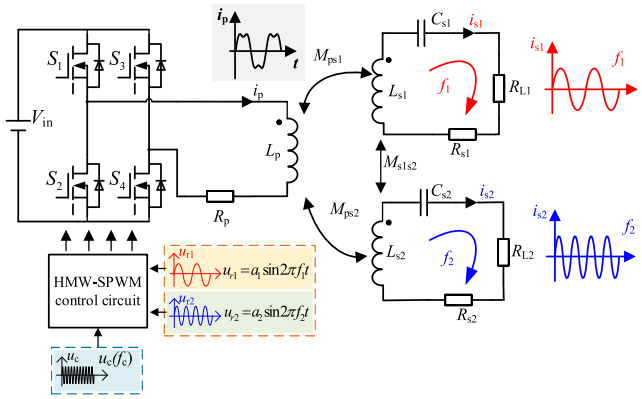

Fig. 3. Structure diagram of a dual-frequency and dual-load MCR-WPT system using HMW-SPWM control method.

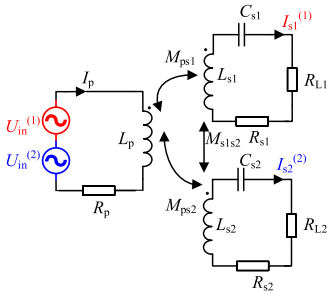

Fig. 4. Equivalent circuit of the dual-frequency and dual-load MCR-WPT system.

According to the working principle and harmonic analysis of the HMW-SPWM control system in Section II, the harmonic effect of the dual-frequency and dual-load MCR-WPT system is very small. Therefore, the equivalent circuit of the dual-frequency and dual-load MCR-WPT system is shown in Fig. 4.

where $U(1)$ in and $U(2)$ in are the rms values of the voltage with frequencies of f_1 and f_2 output by the inverter, as shown in the following:

$$\begin{cases} U_{\text{in}}^{(1)} = \frac{a_1 \cdot V_{\text{in}}}{\sqrt{2}} \\ U_{\text{in}}^{(2)} = \frac{a_2 \cdot V_{\text{in}}}{\sqrt{2}}. \end{cases} \tag{4}$$

Based on the principle of power superposition, the circuit shown in Fig. 4 can be equivalent to the circuit model shown in Fig. 5.

Based on Kirchhoff's voltage law, combined with Fig. 5, the voltage–current relationship matrix can be expressed as

$$\begin{bmatrix} U_{\text{in}}^{(i)} \\ 0 \\ 0 \end{bmatrix} = \begin{bmatrix} Z_p^{(i)} & -j\omega_i M_{ps1} & -j\omega_i M_{ps2} \\ -j\omega_i M_{ps1} & Z_{s1}^{(i)} & j\omega_i M_{s1s2} \\ -j\omega_i M_{ps2} & j\omega_i M_{s1s2} & Z_{s2}^{(i)} \end{bmatrix} \cdot \begin{bmatrix} I_p^{(i)} \\ I_{s1}^{(i)} \\ I_{s2}^{(i)} \end{bmatrix}. \tag{5}$$

Among them, $i = 1, 2$, which, respectively, represent two frequencies f_1, f_2 or two receiving loops or loads. ω_i, $Zp^{(i)}$, ${Z_{s1}}^{(i)}$ ${Z_{s2}}^{(i)}$ are, respectively, the angular frequency of the receiver i, the input impedance of the transmitter and receiver, which can

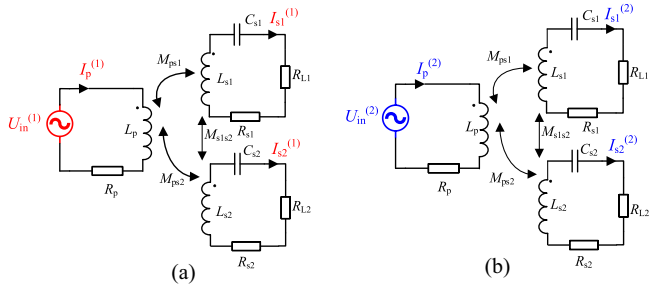

Fig. 5. Simplified circuit model of a dual-frequency and dual-load MCR-WPT system using superposition method. (a) $U(1)$ in acting alone. (b) $U(2)$ in acting alone.

be expressed as

$$\begin{cases} Z_p^{(i)} = R_p + j\omega_i L_p \\ Z_{s1}^{(i)} = R_{s1} + R_{L1} + j\left(\omega_i L_{s1} - 1/\omega_i C_{s1}\right) \\ Z_{s2}^{(i)} = R_{s2} + R_{L2} + j\left(\omega_i L_{s2} - 1/\omega_i C_{s2}\right) \end{cases} \tag{6}$$

where

$$\omega_i = 2\pi f_i. \tag{7}$$

B. Analysis for Power and Efficiency

According to the study in part A, Section III, the power and efficiency characteristics of the dual-frequency and dual-load system are analyzed. Solving (5), the current ${I_p}^{(i)}$ of the transmitting circuit and the currents ${I_{s1}}^{(i)}$ and ${I_{s2}}^{(i)}$ of the two receiving circuits in the system can be calculated as follows:

$$\begin{cases} I_p^{(i)} = \frac{U_{\text{in}}^{(i)}}{Z_{\text{in}}^{(i)}} \\ I_{s1}^{(i)} = \frac{\omega_i^2 M_{ps2} M_{s1s2} + j\omega_i M_{ps1} Z_{s2}^{(i)}}{Z_{s1}^{(i)} Z_{s2}^{(i)} + (\omega_i M_{s1s2})^2} I_{\text{p}}^{(i)} \\ I_{s2}^{(i)} = \frac{\omega_i^2 M_{ps1} M_{s1s2} + j\omega_i M_{ps2} Z_{s1}^{(i)}}{Z_{s1}^{(i)} Z_{s2}^{(i)} + (\omega_i M_{s1s2})^2} I_{\text{p}}^{(i)}. \end{cases} \tag{8}$$

Then, the input impedance of the system can be expressed as

$$\begin{aligned} {Z_{\text{in}}}^{(i)} &= \frac{U_{\text{in}}^{(i)}}{{I_p}^{(i)}} \\ &= {Z_p}^{(i)} + \frac{\omega_i^2 \left({M_{ps1}}^2 Z_{s2}^{(i)} + {M_{ps2}}^2 Z_{s1}^{(i)} \right) - j2\omega_i^3 M_{ps1} M_{ps2} M_{s1s2}}{Z_{s1}^{(i)} Z_{s2}^{(i)} + (\omega_i M_{s1s2})^2}. \end{aligned} \tag{9}$$

Since the modulation waves with two different frequencies are combined to control the high-frequency inverter, the inverter output voltage is equivalent to the superposition of sinusoidal voltages with two different frequencies, so the inductive power of each receiving circuit satisfies the superposition theorem. Therefore, the output power components ${P_{o1}}^{(i)}$ and ${P_{o2}}^{(i)}$ of each receiving circuit and the total output power P_{o1} and P_{o2} of each receiving circuit can be obtained as

$$\begin{cases} P_{o1}^{(i)} = \left| I_{s1}^{(i)} \right|^2 R_{L1} = \left| \frac{U_{in}^{(i)} (\omega_i^2 M_{ps2} M_{s1s2} + j\omega_i M_{ps1} Z_{s2}^{(i)})}{Z_{in}^{(i)} [Z_{s1}^{(i)} Z_{s2}^{(i)} + (\omega_i M_{s1s2})^2]} \right|^2 R_{L1} \\ P_{o2}^{(i)} = \left| I_{s2}^{(i)} \right|^2 R_{L2} = \left| \frac{U_{in}^{(i)} (\omega_i^2 M_{ps1} M_{s1s2} + j\omega_i M_{ps2} Z_{s1}^{(i)})}{Z_{in}^{(i)} [Z_{s1}^{(i)} Z_{s2}^{(i)} + (\omega_i M_{s1s2})^2]} \right|^2 R_{L2} \end{cases} \tag{10}$$

$$\begin{cases} P_{o1} = P_{o1}^{(1)} + P_{o1}^{(2)} \\ P_{o2} = P_{o2}^{(1)} + P_{o2}^{(2)} \end{cases} \tag{11}$$

where $P_{o1}{}^{(1)}$ and $P_{o1}{}^{(2)}$ represent, respectively, the output power components corresponding to the working frequencies f_1 and f_2 in the receiving circuit 1, and P_{o1} represents the total output power of the receiving circuit 1. $P_{o2}{}^{(1)}$ and $P_{o2}{}^{(2)}$ represent, respectively, the output power components corresponding to the working frequencies f_1 and f_2 in the receiving circuit 2, and P_{o2} represents the total output power of the receiving circuit 2.

The power loss of the transmitter and receivers is mainly the internal resistance loss of the transmitting and receiving coils. The power loss component $P_{\text{loss}}{}^{(i)}$ at each frequency and the power loss P_{loss} of the transmitter and receivers are, respectively,

$$P_{\text{loss}}^{(i)} = \left(I_p^{(i)}\right)^2 R_p + \left(I_{s1}^{(i)}\right)^2 R_{s1} + \left(I_{s2}^{(i)}\right)^2 R_{s2} \tag{12}$$

$$P_{\text{loss}} = P_{\text{loss}}^{(1)} + P_{\text{loss}}^{(2)} \tag{13}$$

where $P_{\text{loss}}{}^{(1)}$ and $P_{\text{loss}}{}^{(2)}$, respectively, represent the power loss components at the working frequencies f_1 and f_2, and P_{loss} is the power loss of the transmitter and receivers.

Combining (10)–(13), the efficiency of the transmitter and receivers can be further expressed as

$$\eta = \frac{P_{\text{out}}}{P_{\text{out}} + P_{\text{loss}}} = \frac{P_{o1} + P_{o2}}{P_{o1} + P_{o2} + P_{\text{loss}}}. \tag{14}$$

IV. Multifrequency and Multiload Interfrequency Interference Suppression Criteria

In order to supply power to two loads with different frequencies, two receiving coils and compensation capacitors meet the requirements of (1). From the analysis of (10)–(14) in Section III, we can see that the output power and efficiency of each receiving circuit are not only closely related to the parameters of the system itself, but also affected by other frequency interference. Therefore, in order to reduce the interfrequency interference of each receiving circuit and realize the independent power control of each load, it is necessary to analyze the parameters design criteria for reducing the interfrequency interference. In addition, for receiving circuits with different resonant frequencies, the coupling between the secondary coils has less influence than that of the primary and secondary coils, and it can usually be ignored. Therefore, only the coupling between the primary and secondary coils will be considered in the subsequent analysis, and the influence of cross-coupling between the secondary coils will not be considered.

A. Analysis of the Influence of Different Frequency Interference on the Induced Current of Each Load

Based on the dual-frequency and dual-load MCR-WPT system controlled by HMW-SPWM shown in Fig. 3, taking the influence of power supply $U^{(1)}{}_{\text{in}}$ at frequency f_1 on the power transfer to the load R_{L2} as an example, the interfrequency interference of the dual-frequency and dual-load MCR-WPT system is analyzed.

1) $U(1)$ in $= 0$, $U(2)$ in acting alone

According to (8), the current $I_p{}^{(2)}$ of the primary side can be expressed as

$$I_P{}^{\Delta 2\Delta} = \frac{U_{\text{in}}{}^{\Delta 2\Delta}}{R_{\text{p}} + \text{j}\omega_2 L_p + \frac{(\omega_2 M_{ps2})^2}{R_{L2}{}'} + \frac{(\omega_2 M_{ps1})^2}{R_{L1}{}' + \text{j}X_{\text{s1}}^{(2)}}} \tag{15}$$

where $R_{L1}{}' = R_{L1} + R_{s1}$, $R_{L2}{}' = R_{L2} + R_{s2}$.

Since the power supply $U^{(2)}{}_{\text{in}}$ acts alone, the receiving circuit 2 resonates. The resonance current $I_{s2}{}^{(2)}$ of the receiving circuit 2 is

$$I_{s2}^{(2)} = \frac{\text{j}\omega_2 M_{ps2}}{R_{L2}{}'} I_P{}^{(2)}. \tag{16}$$

2) $U(2)$ in $= 0$, $U(1)$ in acting alone

In the same way, according to (8), the current $I_p{}^{(1)}$ of the primary side can be expressed as

$$I_P{}^{(1)} = \frac{U_{\text{in}}^{(1)}}{R_{\text{p}} + \text{j}\omega_1 L_p + \frac{(\omega_1 M_{ps1})^2}{R_{L1}{}'} + \frac{(\omega_1 M_{ps2})^2}{R_{L2}{}' + \text{j}X_{\text{s2}}^{(1)}}}. \tag{17}$$

Since the power supply $U(1)$ in acts alone, the receiving circuit 2 does not resonate, and the interference current $I_{s2}{}^{(1)}$ of the receiving circuit 2 is

$$I_{s2}^{(1)} = \frac{\text{j}\omega_1 M_{ps2} I_P{}^{\Delta 1\Delta}}{R_{L2}{}' + \text{j}\text{X}_{s2}{}^{(1)}}. \tag{18}$$

B. Interfrequency Interference Suppression Criterion

In order to analyze the interference of different frequencies power supply to the loads, the interference current $I_{s2}{}^{(1)}$ of the receiving circuit 2 and the resonance current $I_{s2}{}^{(2)}$ are compared, as shown in the following:

$$\begin{aligned} \left|\frac{I_{s2}^{(1)}}{I_{s2}^{(2)}}\right| &= \left| \frac{\frac{a_1\omega_1}{a_2\omega_2} \cdot \frac{R_{L2}{}'}{R_{L2}{}' + \text{j}\text{X}_{s2}{}^{(1)}}}{\cdot \frac{R_p + \text{j}\omega_2 L_p + \frac{(\omega_2 M_{ps2})^2}{R_{L2}{}'} + \frac{(\omega_2 M_{ps1})^2}{R_{L1}{}' + \text{j}X_{\text{s1}}^{(2)}}}{R_p + \text{j}\omega_1 L_p + \frac{(\omega_1 M_{ps1})^2}{R_{L1}{}'} + \frac{(\omega_1 M_{ps2})^2}{R_{L2}{}' + \text{j}X_{s2}^{(1)}}}} \right| \\ &= m \cdot \left| \frac{1}{1 + \text{j}\frac{\text{X}_{s2}{}^{(1)}}{R_{L2}{}'}} \right| = \frac{m}{\sqrt{1 + \left(\frac{\text{X}_{s2}{}^{(1)}}{R_{L2}{}'}\right)^2}} \end{aligned} \tag{19}$$

where

$$m = \left| \frac{a_1\omega_1}{a_2\omega_2} \cdot \frac{R_p + \text{j}\omega_2 L_p + \frac{(\omega_2 M_{ps2})^2}{R_{L2'}} + \frac{(\omega_2 M_{ps1})^2}{R_{L1'} + \text{j}X_{\text{s1}}^{(2)}}}{R_p + \text{j}\omega_1 L_p + \frac{(\omega_1 M_{ps1})^2}{R_{L1'}} + \frac{(\omega_1 M_{ps2})^2}{R_{L2'} + \text{j}X_{s2}^{(1)}}} \right| (m > 0). \tag{20}$$

To reduce the current distortion of the receiving circuit 2, it is necessary to ensure that the resonance current $I_{s2}{}^{(2)}$ of the receiving circuit 2 remains unchanged and the interference current $I_{s2}{}^{(1)}$ should be reduced. When it is satisfied that the proportion of the interference current $I_{s2}{}^{(1)}$ in the resonance current $I_{s2}{}^{(2)}$ of the receiving circuit 2 does not exceed 5%, that

is

$$\left|\frac{I_{s2}^{(1)}}{I_{s2}^{(2)}}\right| = \frac{m}{\sqrt{1+\left(\frac{X_{s2}{}^{(1)}}{R_{L2}{}'}\right)^2}} \le 5\%. \tag{21}$$

According to (21), the inductance of the receiving coil is increased to improve the frequency selection characteristic of the receiving circuit and reduce the interfrequency interference of the system. In this case, the directional transfer requirements of specific frequency energy to the target load can be met, and the independent and controllable wireless power supply for multiple loads can be realized.

V. Performance Analysis of Multifrequency and Multiload MCR-WPT System Using HMW-SPWM Control Method

It can be seen from the analysis in Sections III and IV, the load resistance and the mutual inductance of the primary and secondary sides have a great influence on the power transfer characteristics of the MFML MCR-WPT system using HMW-SPWM control method. Therefore, it is necessary to analyze them to select the appropriate system parameters to improve the power transfer capacity and the efficiency of the loads with different frequencies.

A. Analysis of Load Characteristics

Based on the criterion of interfrequency interference suppression, the output power of receiving circuit *i* is approximately

$$P_{\mathrm{out}i} = |I_{si}|^2 R_{Li} = \left|\frac{\mathrm{j}\omega_i M_{\mathrm{psi}} \cdot I_p^{(i)}}{Z_{si}^{(i)}}\right|^2 R_{Li}. \tag{22}$$

According to (22), if a receiving circuit is misaligned, that is, the mutual inductance M_{psi} changes, the output power of the corresponding receiving circuit also changes, but the output power of other receiving circuits will almost not be affected.

According to (6), (8), and (22), the output power of receiving circuit *i* is further written as

$$P_{\mathrm{out}i} = \left|\frac{\mathrm{j}\omega_i M_{\mathrm{psi}}}{\sqrt{2}R_{Li}{}'} \cdot \frac{a_i V_{\mathrm{in}}}{R_p + \mathrm{j}\omega_i L_p + \frac{(\omega_i M_{psi})^2}{R_{Li}{}'}}\right|^2 R_{Li}. \tag{23}$$

According to (23), the output power $P_{\mathrm{out}i}$ of the receiving circuit *i* is also related to the amplitude a_{i} of the modulation wave and the load R_{Li}. The output power of the receiving circuit changes with the corresponding modulation amplitude or load, but it basically has no influence on other receiving circuits.

In order to further analyze the relationship between the output power $P_{\mathrm{out}i}$ and the load R_{Li}, in the case that other parameters remain unchanged, the output power $P_{\mathrm{out}i}$ of the receiving circuit *i* has a maximum value when the load R_{Li} changes.

Making

$$\frac{\mathrm{d}P_{\mathrm{out}i}}{\mathrm{d}R_{Li}} = 0 \tag{24}$$

the theoretical optimal load R_{Li} corresponding to the maximum output power of receiving circuit *i* can be obtained as

$$R_{Li} = \frac{{\omega_i}^2 {M_{psi}}^2}{\sqrt{{R_p}^2 + {\omega_i}^2 {L_p}^2}}. \tag{25}$$

Under this optimal load R_{Li}, the maximum output power of receiving circuit *i* can be obtained as

$$(P_{\mathrm{out}i})_{\max} = \frac{{a_i}^2 {V_{\mathrm{in}}}^2}{4(R_p + \sqrt{{R_p}^2 + {\omega_i}^2 {L_p}^2})}. \tag{26}$$

From (25) and (26), it can be concluded that when the mutual inductance of the transmitting and receiving coils and the load resistance meet (25), the maximum output power of the receiving circuit *i* can be guaranteed. The maximum output power of the receiving circuit *i* is mainly determined by the dc voltage source V_{in}, the amplitude a_i of the modulation wave, the inductance L_p of the primary coil and its internal resistance R_p, and the resonance frequency ω_i of the receiving circuit *i*. Under the premise of ensuring the independent and reliable power transfer of different frequencies, for a given frequency, increasing the dc voltage of the primary system, the amplitude of the modulation wave, and reducing the inductance of the transmitting coil and its internal resistance can correspondingly increase the maximum output power of the receiving circuit. Therefore, in the experimental parameter design of the system, the relevant parameters of the system can be optimized according to the above characteristics.

B. Power Factor and Efficiency Analysis

As shown in Fig. 3, since there is no compensation network in the primary circuit, there must be a certain amount of reactive power in the system. For a dual-frequency and dual-load MCR-WPT system, under the premise of meeting the interfrequency interference suppression criterion, according to (10)–(13), the active power of the system is

$$\begin{aligned} P &= P_{\mathrm{out}} + P_{\mathrm{loss}} \\ &= P_{o1} + P_{o2} + P_{\mathrm{loss}}^{(1)} + P_{\mathrm{loss}}^{(2)}. \end{aligned} \tag{27}$$

According to (8), the reactive power of the system is

$$Q = \left|I_p^{(1)}\right|^2 \omega_1 L_p + \left|I_p^{(2)}\right|^2 \omega_2 L_p. \tag{28}$$

So, the power factor of the system can be expressed as (29):

$$\mathrm{PF} = \frac{P}{\sqrt{P^2 + Q^2}}. \tag{29}$$

Since the mutual inductance M_{psi} between transmitting and receiving coils is proportional to the coupling coefficient k_i, when the interfrequency interference suppression criterion is met, some parameters in Table I are $V_{\mathrm{in}} = 48$ V, $f_1 = 20$ kHz, $f_2 = 60$ kHz, $L_p = 29.1$ μH, $L_{\mathrm{s1}} = 88.6$ μH, $L_{\mathrm{s2}} = 89.1$ μH, $R_p = 0.05$ Ω, $R_{s1} = 0.08$ Ω, $R_{s2} = 0.08$ Ω, $C_{s1} = 691.8$ nF, $C_{s2} = 74.95$ nF, $R_{L1} = 1$ Ω, and $R_{L2} = 5$ Ω. Based on (27)–(29), the relationship among the power factor, coupling coefficients k_1 and k_2 of the primary and secondary sides is shown in Fig. 6(a).

TABLE I
SYSTEM PARAMETERS

Parameter		Symbol	Value	Parameter		Symbol	Value
Input voltage		V_{in}	48V	Case 1	Capacitor of Receiver-2	C_{s2}	74.95nF
Inductance of transmitter		L_p	29.1μH	Case 2	Working frequency	f_1	20kHz
ESR of L_p		R_p	0.05Ω			f_2	80kHz
Inductance of Receiver-1		L_{s1}	88.6μH		Capacitor of Receiver-1	C_{s1}	691.8nF
ESR of L_{s1}		R_{s1}	0.08Ω		Capacitor of Receiver-2	C_{s2}	47.5nF
Mutual inductance 1		M_{ps1}	17.1μH	Carrier frequency		f_c	600kHz
Inductance of Receiver-2		L_{s2}	89.1μH	Transmitt -ing coil	Outer diameter	De_p	26cm
ESR of L_{s2}		R_{s2}	0.08Ω		Turns	N_p	9
Mutual inductance 2		M_{ps2}	16.6μH	Receiving coil-1	Outer diameter	De_{s1}	26cm
Load	Receiver-1	R_{L1}	1Ω		Turns	N_{s1}	21
	Receiver-2	R_{L2}	5Ω	Receiving coil-2	Outer diameter	De_{s2}	26cm
Case 1	Working frequency	f_1	20kHz		Turns	N_{s2}	21
		f_2	60kHz	Distance	Transmitter to Receiver-1	d_{ps1}	6cm
	Capacitor of Receiver-1	C_{s1}	691.8nF		Transmitter to Receiver-2	d_{ps2}	7cm

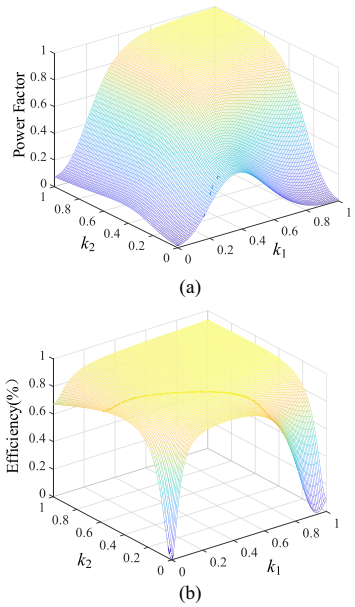

Fig. 6. Surfaces of power factor and efficiency. (a) Power factor. (b) Efficiency.

Based on (14), the relationship among the efficiency, coupling coefficients k_1 and k_2 of the primary and secondary sides is shown in Fig. 6(b).

Fig. 6 depicts that the power factor and efficiency improve gradually when the coupling coefficients of the primary and secondary sides increase. Therefore, in the process of parameter design, while other design requirements are met, appropriately increasing the coupling coefficients of the system can effectively improve the power factor and efficiency.

C. Analysis of Dynamic Characteristics

For more intuitively describing the independent control performance of the system, the transient response of the output currents is analyzed. When the modulation amplitude a_1 changes and the modulation amplitude a_2 remains constant, the transient responses of the output currents of the receiving circuits with different frequencies are shown in Fig. 7.

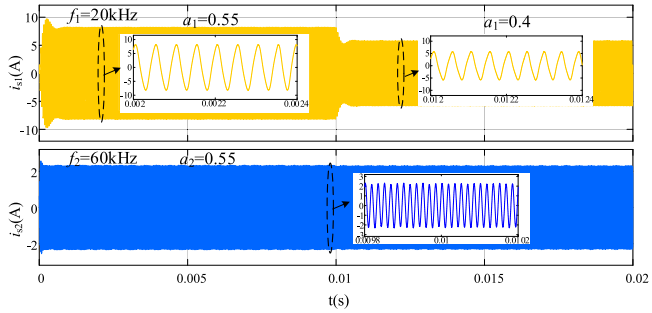

Fig. 7. Transient responses of the output currents of the receiving circuits with different frequencies.

It can be seen from Fig. 7 that if the modulation amplitude a_1 changes while the modulation amplitude a_2 remains unchanged during the runtime, the output current of the receiving circuit 1 will change correspondingly, and the output current of the receiving circuit 2 will be basically unaffected. Therefore, the independent control of the output power with different frequencies can be realized in the dual-frequency and dual-load MCR-WPT system.

In addition, in order to describe the system model in a certain range of frequency domain, the frequency responses of the system are analyzed. According to the system parameters design criteria, system parameters are given in Table I.

Based on the dual-frequency and dual-load MCR-WPT system and relevant parameters, the transfer function G_1 of the system receiving circuit 1 and the transfer function G_2 of the system receiving circuit 2 are obtained, which are, respectively

$$G_1 = \frac{u_1(s)}{u_0(s)} = \frac{8449.35s^4+4.82e8s^3+1.27e15s^2}{s^5+80891s^4+1.89943e11s^3+3.89607e15s^2+3.13642e21s+5.37518e24} \tag{30}$$

$$G_2 = \frac{u_2(s)}{u_0(s)} = \frac{40975.5s^4+4.99e8s^3+6.68e14s^2}{s^5+80891s^4+1.89943e11s^3+3.89607e15s^2+3.13642e21s+5.37518e24} \tag{31}$$

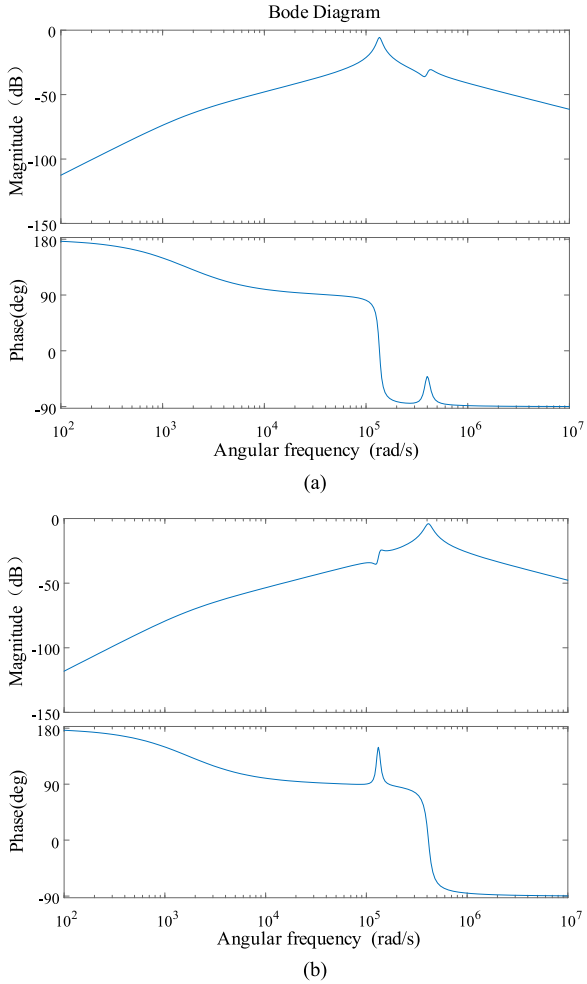

Fig. 8. Frequency response of the system circuits. (a) Frequency response of the system receiving circuit 1 ($f_1 = 20$ kHz). (b) Frequency response of the system receiving circuit 2 ($f_2 = 60$ kHz).

where $u_0(s)$ is the power supply voltage, $u_1(s)$ is the output voltage of the receiving circuit 1, and $u_2(s)$ is the output voltage of the receiving circuit 2.

According to (30) and (31), the frequency responses of the system receiving circuits are, respectively, drawn. Fig. 8(a) is the frequency response of the system receiving circuit 1, whose resonant frequency is 20 kHz. Fig. 8(b) is the frequency response of the system receiving circuit 2, whose resonant frequency is 60 kHz.

It can be seen from Fig. 8(a) and (b) that when the working frequency of the system is consistent with the resonant frequency of the receiving circuit, the amplitude is the maximum. In addition, when the working frequency corresponding to the angular frequency of the system is 60 kHz in Fig. 8(a) or 20 kHz in Fig. 8(b), the amplitude-frequency response of the transfer function G_1 or G_2 increases slightly, and the increase in phase angle is relatively obvious. In general, it has little effect on the power transfer of the target frequency.

For the target frequency power transfer, the receiving circuit has good transmission characteristics, which has good suppression effect on the interfrequency interference to realize the directional power transfer to the target load.

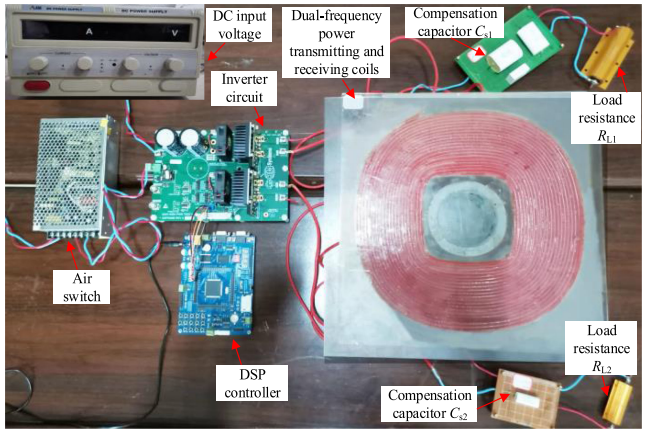

Fig. 9. Dual-frequency and dual-load experimental platform.

VI. Simulation and Experimental Verification

In order to verify the validity of the theoretical analysis and the feasibility of the proposed method, a dual-frequency and dual-load experimental platform is built, as shown in Fig. 9. The system includes the control circuit board, the full-bridge inverter, the transmitting coil and the receiving coils, the compensation capacitors, loads, etc. The receiving coils are placed on both sides of the transmitting coil to reduce cross-coupling. The carrier frequency is set to 600 kHz, which is also the switching frequency of the inverter. Therefore, the gallium nitride inverter platform is adopted to ensure the generation of high-frequency power, and its driving pulses are generated by the DSP28335 and amplified by the driving circuit. In addition, the dead time is set to 60 ns to prevent the transistor straight up and down and avoid waveform distortion.

Since the carrier frequency of the HMW-SPWM control circuit is 600 kHz, in order to avoid waveform distortion, the receiving circuit with working frequency of 20 and 60 kHz or 20 and 80 kHz are chosen for technical verification.

A. Independent Control Verification of the Dual-Frequency and Dual-Load MCR-WPT System

When the resonant frequencies of the receiving circuits are 20 and 60 kHz, respectively, based on Table I, if the amplitudes a_1 and a_2 of the two modulation waves are set to 0.55, the simulation waveforms of the inverter output voltage and current are shown in Fig. 10, and their Fast Fourier Transformation (FFT) spectrums analysis are demonstrated in Fig. 11. The experimental waveforms of the inverter output voltage and current are shown in Fig. 12.

According to Figs. 10 and 11, it can be seen that the inverter output voltage is the high-frequency hybrid pulse voltage, and the inverter output current is equivalent to the superposition of 20 kHz current and 60 kHz current components. From Fig. 12,

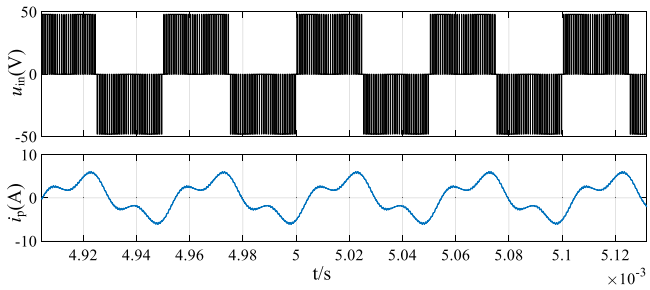

Fig. 10. Simulation waveforms of the inverter output voltage and current. (a) Voltage spectrum. (b) Current spectrum.

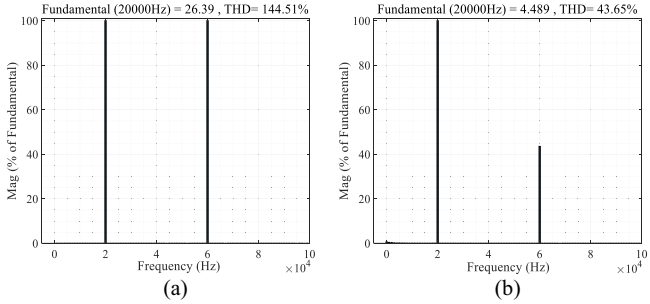

Fig. 11. Inverter output voltage and current spectrum analysis.

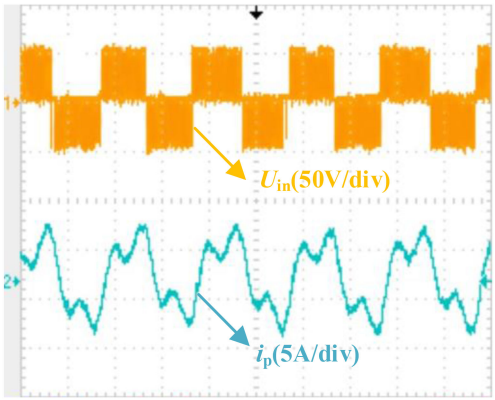

Fig. 12. Experimental waveforms of the inverter output voltage and current.

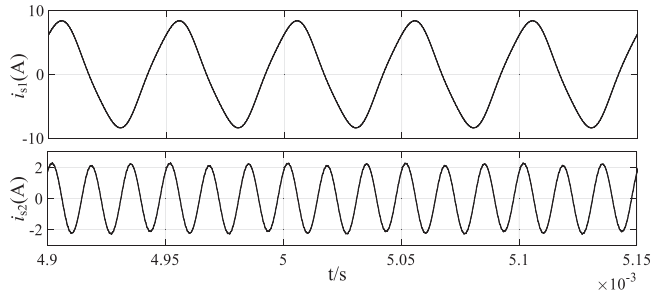

Fig. 13. Simulation current waveforms of two receiving circuits when $f_1 = 20$ kHz and $f_2 = 60$ kHz based on the original circuit configuration. (a) Current spectrum ($f_1 = 20$ kHz). (b) Current spectrum ($f_2 = 60$ kHz).

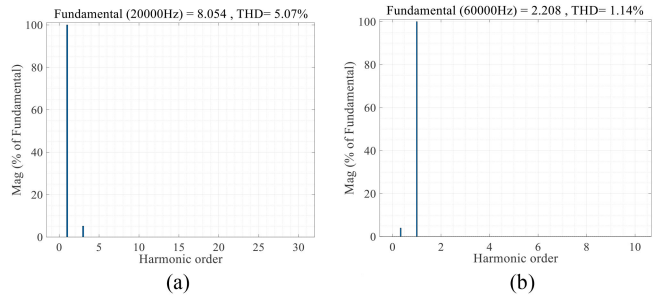

Fig. 14. Current FFT spectrums analysis of two receiving circuits based on the original circuit configuration.

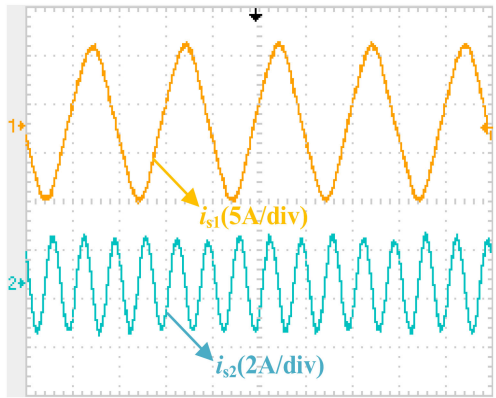

Fig. 15. Experimental current waveforms of two receiving circuits when $f_1 = 20$ kHz and $f_2 = 60$ kHz based on the original circuit configuration.

it is verified that the dual-frequency power output of the inverter can be realized by HMW-SPWM control method.

Based on the original proposed circuit configuration in Fig. 3, if the amplitudes a_1 and a_2 of the two modulation waves are both 0.55, the simulation waveforms of two receiving circuits with resonant frequencies of $f_1 = 20$ kHz and $f_2 = 60$ kHz are, respectively, shown in Fig. 13. In order to verify the effectiveness of the power transfer with different frequencies, the FFT spectrums analysis of two receiving circuits is shown in Fig. 14. The experimental waveforms of two receiving circuits with resonant frequencies of $f_1 = 20$ kHz and $f_2 = 60$ kHz are shown in Fig. 15.

In Figs. 13 and 15, the simulation current waveforms of the two receiving circuits with resonant frequencies of $f_1 = 20$ kHz and $f_2 = 60$ kHz are basically the same as the experimental waveforms. The current spectrum analysis in Fig. 14 shows that the current distortions are acceptable, and the feasibility of the proposed system is initially verified.

For more intuitively describing the independent and dynamic control performance of the system, the amplitude a_1 of the modulation wave is set to reduce from 0.55 to 0.4 and the amplitude a_2 of the modulation wave remains unchanged at 0.55 during the runtime. Fig. 16(a) shows that the experimental current waveforms of two receiving circuits under the modulation amplitude variation. In addition, it is also necessary to verify the transient current response of the receiving circuits under the load variation. The load R_{L2} is set to increase from 5 to 8 Ω and the load R_{L1} remains unchanged at 1 Ω. Fig. 16(b) shows the

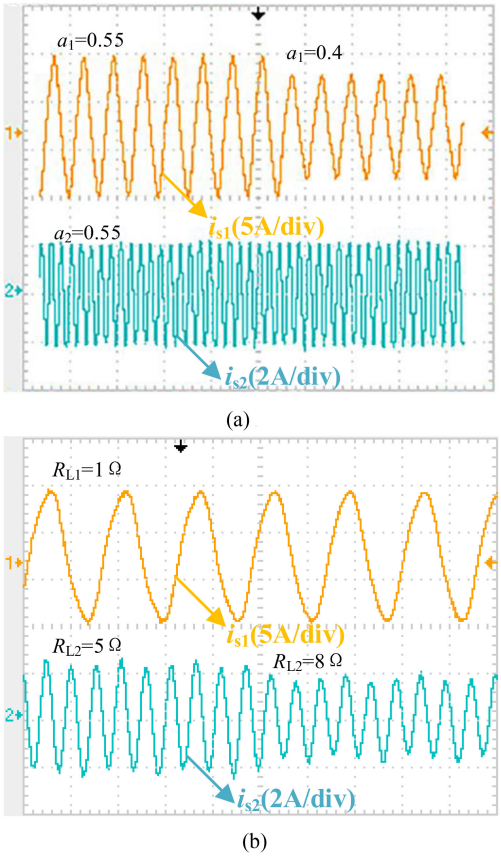

Fig. 16. Experimental transient current waveforms of two receiving circuits. (a) Modulation amplitude variation. (b) Load variation.

TABLE II
OUTPUT POWER OF THE RECEVING CIRCUITS AND A_2

a_2 / P_{out}(W)	0.4	0.45	0.5	0.55	0.6	0.65
P_{out1}	14.8	14.8	14.9	14.9	14.9	14.9
P_{out2}	6	7.5	9	11	13	15.4

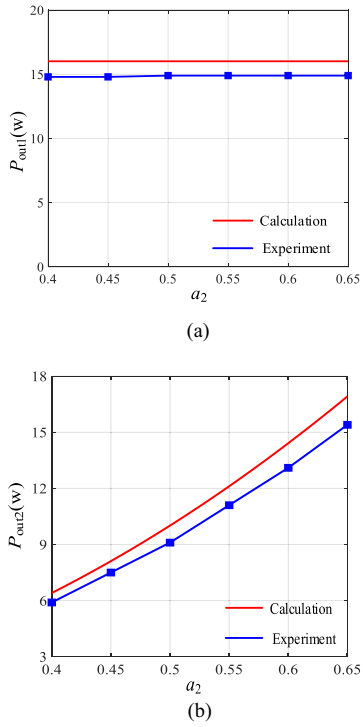

Fig. 17. Calculations and experiments of the output power of the receiving circuits with different resonant frequencies changing with the amplitude a_2 of the modulation wave. (a) $P_{\mathrm{out}1}$ and a_2. (b) $P_{\mathrm{out}2}$ and a_2.

experimental current waveforms of two receiving circuits under the load variation.

It can be seen from Fig. 16(a) that if the amplitude a_1 of the modulation wave is reduced and the amplitude a_2 of the modulation wave keeps unchanged during the runtime, the current value of receiving circuit 1 is correspondingly reduced, and the current value of receiving circuit 2 remains unchanged.

Similarly, if the load R_{L2} increases and the load R_{L1} remains constant during the runtime, the current value of receiving circuit 2 is correspondingly reduced, and the current value of receiving circuit 1 is almost unaffected, thus verifying that the output power of the dual-frequency and dual-load MCR-WPT system is independent and controllable.

The amplitude a_1 of the modulation wave keeps unchanged at 0.4, and the amplitude a_2 of the modulation wave is set to vary from 0.4 to 0.65, and the current values of the two receiving circuits with resonant frequencies of $f_1 = 20$ kHz and $f_2 = 60$ kHz are recorded. According to experimental data of different receiving circuit currents, Table II shows the output power of the receiving circuits with different resonant frequencies varying with the amplitude a_2 of the modulation wave.

The calculations and experiments of the output power of the receiving circuits with different resonant frequencies changing with the amplitude a_2 of the modulation wave are shown in Fig. 17.

It can be seen from Fig. 17(a) and (b) that when the amplitude a_2 of the modulation wave changes, the output power of the receiving circuit 1 basically remains unchanged, and the output power of the receiving circuit 2 gradually improves with the increase of the amplitude a_2 of the modulation wave. Therefore, adjusting the amplitude of the modulation wave within a certain range can meet different power requirements of the target load without affecting the power transfer at other frequencies, thereby realizing the independent and controllable wireless power supply requirements of different power levels and multiple loads.

The efficiency of the system mainly includes two aspects, one is the efficiency of the inverter and the other is the efficiency of the transmitter and receivers. Fig. 18 shows calculations and experiments results of the efficiency of the transmitter and receivers changing with the amplitude a_2 of the modulation wave.

In Fig. 18, under the premise of ensuring the reliable operation of the system, when the amplitude a_2 of the modulation wave changes, the efficiency of the transmitter and receivers always remains above 85%.

In Figs. 17 and 18, the reasons for the differences in the simulations and measurements are mainly due to the loss of the

TABLE III
PERFORMANCE COMPARISON

	Power(W)	Efficiency(%)	Transmission mechanism	Number of inverters	Independent power control
[17]	70	75	Simultaneous	Multiple	No
[18]	7.4	70.6	Simultaneous	Multiple	No
[21]	n/a	24~29	Time-sharing	Single	Yes
This work	40	65~70	Simultaneous	Single	Yes

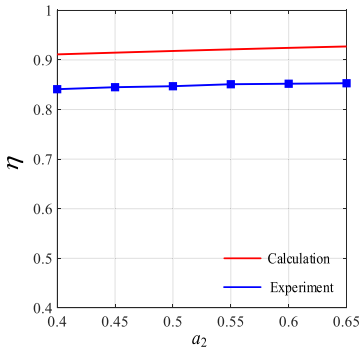

Fig. 18. Calculations and experiments results of the efficiency of the transmitter and receivers changing with the amplitude a_2 of modulation wave.

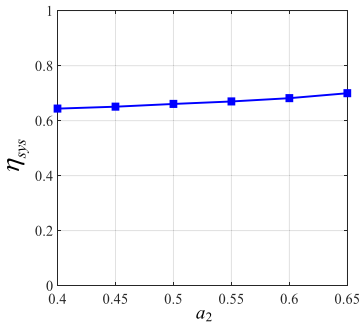

Fig. 19. Experimental results of the total system efficiency changing with the amplitude a_2 of the modulation wave.

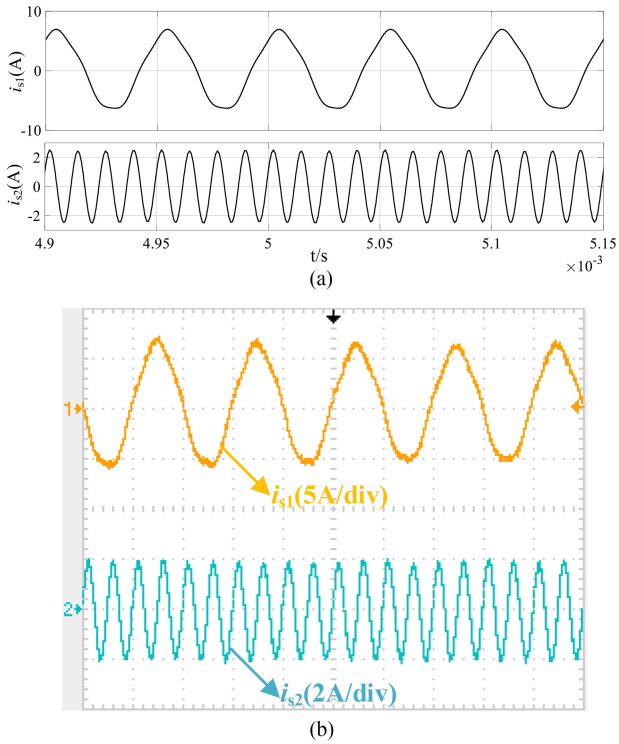

Fig. 20. Simulation and experimental current waveforms of two receiving circuits when $f_1 = 20$ kHz and $f_2 = 80$ kHz based on the original circuit configuration. (a) Simulation waveforms. (b) Experimental waveforms.

inverter, the measurement error of the components and the loss of internal resistance. In the following research, the high-frequency inverter with better performance and more precise measuring instruments will be sought to reduce errors.

In addition, the loss of high-frequency inverter is also worthy of attention. In the experiment, the efficiency of the inverter is measured, and the total system efficiency is

$$\eta_{\text{sys}} = \eta_i \cdot \eta \tag{32}$$

where η is the efficiency of the transmitter and receivers, η_{i} is the inverter efficiency, and η_{sys} is the total system efficiency.

The experimental results of the total system efficiency changing with the amplitude a_2 of the modulation wave are shown in Fig. 19.

To illustrate the superior performance of the proposed HMW-SPWM methodology in this article, Table III summarizes the performance of the proposed system in comparison to prior art.

As shown in Table III, the comparison has been carried out in the perspective of system performance, transmission mechanism, number of inverters, independent power control, etc. In [17] and [18], multiple inverters are adopted to supply power for multiple loads with different frequencies simultaneously, and the efficiency reaches more than 70%. However, the independent control of multifrequency power cannot be realized in the system. In [21], the system uses a single inverter to supply power for loads with different frequencies and realizes independent control of multifrequency power. However, it cannot supply power for loads with different frequencies simultaneously and the system efficiency is low.

In this article, due to only one inverter and one transmitting coil in the proposed scheme, the topology has a compact size and low weight; meanwhile, it can also achieve simultaneous power transfer to loads with different frequencies and independent power control by adjusting the frequency and amplitude of the modulation wave appropriately. However, it is worth mentioning

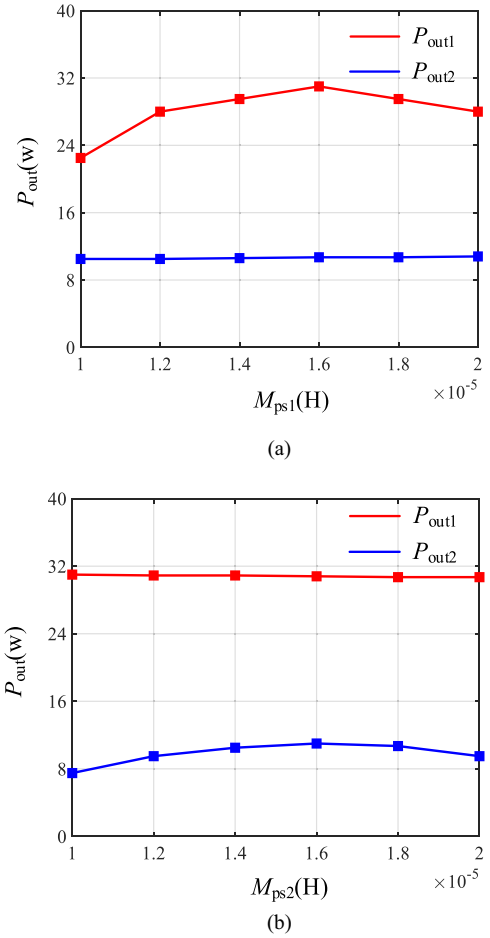

Fig. 21. Misalignment between the transmitter and the receivers. (a) Misalignment between the transmitter and the receiver-1. (b) Misalignment between the transmitter and the receiver-2.

that the efficiency of the system is not very high. In the future, the corresponding reactive power compensation network will be designed to reduce the inverter loss and realize efficient power transfer of the system.

B. Power Transfer Verification With Frequency Variation

In order to verify power transfer with frequency variation, the resonant frequencies of the receiving circuit are adjusted to 20 and 80 kHz, respectively, whereas other parameters of the system remain unchanged. The amplitudes of two modulation waves are both set to 0.45 and the capacitance of the receiving circuit 2 are rematched. The simulation and experimental current waveforms of two receiving circuits with resonant frequencies of $f_1 = 20$ and $f_2 = 80$ kHz are shown in Fig. 20.

It can be seen from Fig. 20 that the current waveforms of the receiving circuits with resonant frequencies of $f_1 = 20$ kHz and $f_2 = 80$ kHz are similar to standard sine waves, which realizes the acquisition of electric energy at target frequencies and can adapt to the power supply requirements of the loads at different working frequencies, thereby realizing MFML wireless power supply compatible.

C. Power Transfer Verification Under Misalignment

Since misalignment is an important factor to be considered in the MCR-WPT system, Fig. 21 shows the variation of output power of two receiving circuits when one of them is misaligned.

According to Fig. 21, when one of the receivers is not aligned with the transmitter, the output power of the corresponding receiving circuit changes, but it has little effect on the other receiving circuit. Therefore, the misalignment between the transmitting coil and the receiving coil in the dual-frequency and dual-load MCR-WPT system using HMW-SPWM control only affects the power transfer of corresponding path, and it has no effect on other paths, ensuring the normal power transfer of other receiving circuits.

VII. Conclusion

To realize independent and controllable wireless power transfer for the MFML MCR-WPT system, the concept of HMW-SPWM is proposed from a new perspective. The MFML MCR-WPT system using HMW-SPWM control method is introduced in this article. Taking a dual-frequency and dual-load MCR-WPT system as an example, the system is modeled, and the HMW-SPWM control circuit was designed to realize multifrequency independent power control. The parameter design criteria are studied to reduce the interference of different frequencies. In addition, the load characteristics and power factor of the system are analyzed to select the appropriate system parameters and optimize the output power of receiving circuits. Furthermore, the dynamic characteristics of the system are analyzed to intuitively describe the independent, reliable power transfer. Finally, experiments are implemented to verify the validity of the theoretical analysis and the feasibility of the proposed method.

However, the method proposed in this article still has the following shortcomings, which need to be further studied.

1) To achieve multifrequency power transfer, the transmitting coil adopts a zero compensation strategy, and there is some reactive power in the system, which increases the system loss. In the future, the reactive power compensation structure and the magnetic circuit mechanism of the system will be further optimized to realize the reliable and efficient multifrequency wireless power transfer.
2) The switching frequency of the inverter is relatively high by using HMW-SPWM control method, the circuit topology should be further improved or new switching devices suitable for higher frequency should be sought to reduce waveforms distortion and transmit power at higher frequencies.

References

[1] Z. Zhang, H. Pang, A. Georgiadis, and C. Cecati, "Wireless power transfer—An overview," *IEEE Trans. Ind. Electron.*, vol. 66, no. 2, pp. 1044–1058, Feb. 2019.

[2] J. Dai and D. C. Ludois, "A survey of wireless power transfer and a critical comparison of inductive and capacitive coupling for small gap applications," *IEEE Trans. Power Electron.*, vol. 30, no. 11, pp. 6017–6029, Nov. 2015.

[3] C. Xia, R. Chen, Y. Liu, L. Liu, and G. Chen, "Inhibition of current harmonics in LCL/LCC wireless power transfer system," in *Proc. IEEE PELS Workshop Emerg. Technol.: Wireless Power Transfer*, 2017, pp. 1–6.

[4] C. Xia, W. Wang, S. Ren, X. Wu, and Y. Sun, "Robust control for inductively coupled power transfer systems with coil misalignment," *IEEE Trans. Power Electron.*, vol. 33, no. 9, pp. 8110–8122, Sep. 2018.
[5] Z. Yan, B. Song, Y. Zhang, K. Zhang, Z. Mao, and Y. Hu, "A rotation-free wireless power transfer system with stable output power and efficiency for autonomous underwater vehicles," *IEEE Trans. Power Electron.*, vol. 34, no. 5, pp. 4005–4008, May 2019.
[6] C. Zhang, N. Tang, W. Zhong, C. K. Lee, and R. S. Y. Hui, "A new energy harvesting and wireless power transfer system for smart grid," in *Proc. IEEE 7th Int. Symp. Power Electron. Distrib. Gener. Syst.*, 2016, pp. 1–5.
[7] Z. Huang, I. W. Iam, I. U. Hoi, C. Lam, P. Mak, and R. P. Martins, "Self-contained solar-powered inductive power transfer system for wireless electric vehicle charging," in *Proc. IEEE PES Asia-Pacific Power Energy Eng . Conf .*, 2019, pp. 1–6.
[8] Z. Nie and Y. Yang, "A model independent scheme of adaptive focusing for wireless powering to in-body shifting medical device," *IEEE Trans. Antennas Propag.*, vol. 66, no. 3, pp. 1497–1506, Mar. 2018.
[9] H. Ju and R. Zhang, "Throughput maximization in wireless powered communication networks," *IEEE Trans. Wireless Commun.*, vol. 13, no. 1, pp. 418–428, Jan. 2014.
[10] M. Fu, T. Zhang, C. Ma, and X. Zhu, "Efficiency and optimal loads analysis for multiple-receiver wireless power transfer systems," *IEEE Trans. Microw. Theory Techn.*, vol. 63, no. 3, pp. 801–812, Mar. 2015.
[11] C. Li, J. Cao, D. Hu, and H. Zhang, "Transmission characteristics of magnetic resonance coupling-based multi-load wireless power transmission system," *J. Eng.*, vol. 2019, no. 13, pp. 132–137, 2019.
[12] C. Cheng, Z. Zhou, W. Li, C. Zhu, Z. Deng, and C. C. Mi, "A multi-load wireless power transfer system with series-parallel-series compensation," *IEEE Trans. Power Electron.*, vol. 34, no. 8, pp. 7126–7130, Aug. 2019.
[13] Z. Zhou *et al.*, "A Multi-load wireless power transfer system with constant voltage outputs using S-LCC compensation," in *Proc. 22nd Int. Conf. Elect. Mach. Syst.*, 2019, pp. 1–6.
[14] Y. Zhang, T. Lu, Z. Zhao, F. He, K. Chen, and L. Yuan, "Employing load coils for multiple loads of resonant wireless power transfer," *IEEE Trans. Power Electron.*, vol. 30, no. 11, pp. 6174–6181, Nov. 2015.
[15] R. Hou, X. Wang, J. Wu, H. Song, and Y. Qu, "Research and application of dual-load wireless power transmission system," in *Proc. 22nd Int. Conf. Elect. Mach. Syst.*, 2019, pp. 1–5.
[16] L. Tan *et al.*, "Power stability optimization design of three-dimensional wireless power transmission system in multi-load application scenarios," *IEEE Access*, vol. 8, pp. 91843–91854, 2020.
[17] F. Liu, Y. Yang, Z. Ding, X. Chen, and R. M. Kennel, "A multi-frequency superposition methodology to achieve high efficiency and targeted power distribution for a multi-load MCR WPT system," *IEEE Trans. Power Electron.*, vol. 33, no. 10, pp. 9005–9016, Oct. 2018.
[18] D. Ahn and P. P. Mercier, "Wireless power transfer with concurrent 200-kHz and 6.78-MHz operation in a single-transmitter device," *IEEE Trans. Power Electron.*, vol. 31, no. 7, pp. 5018–5029, Jul. 2016.
[19] X. Zhang, F. Liu, and T. Mei, "Multifrequency phase-shifted control for multiphase multiload MCR WPT system to achieve targeted power distribution and high misalignment tolerance," *IEEE Trans. Power Electron.*, vol. 36, no. 1, pp. 991–1003, Jan. 2021.
[20] C. Zhao and D. Costinett, "GaN-based dual-mode wireless power transfer using multi-frequency programmed pulse width modulation," *IEEE Trans. Ind. Electron.*, vol. 64, no. 11, pp. 9165–9176, Nov. 2017.
[21] Y. Kim, D. Ha, W. J. Chappell, and P. P. Irazoqui, "Selective wireless power transfer for smart power distribution in a miniature-sized multiple-receiver system," *IEEE Trans. Ind. Electron.*, vol. 63, no. 3, pp. 1853–1862, Mar. 2016.
[22] W. Li, J. Lu, G. Zhu, W. Zhang, and J. Jiang, "Design and research of a double-sided flux coupler in inductive power transfer system," in *–Proc. 42nd Annu. Conf. IEEE Ind. Electron. Soc.*, 2016, pp. 6033–6037.
[23] B. Yang, W. Li, Y. Gu, W. Cui, and X. He, "Improved transformerless inverter with common-mode leakage current elimination for a photovoltaic grid-connected power system," *IEEE Trans. Power Electron.*, vol. 27, no. 2, pp. 752–762, Feb. 2012.
[24] L. Qin, M. Hu, D. D. Lu, Z. Feng, Y. Wang, and J. Kan, "Buck–boost dual-leg-integrated step-up inverter with low THD and single variable control for single-phase high-frequency AC microgrids," *IEEE Trans. Power Electron.*, vol. 33, no. 7, pp. 6278–6291, Jul. 2018.

Chenyang Xia (Member, IEEE) was born in Jiangsu Province, China, in 1982. He received the B.S., M.S., and Ph.D. degrees in control theory and control engineering from Chongqing University, Chongqing, China, in 2006, 2008, and 2010, respectively.

From 2018 to 2019, he was an Academic Visitor with the University of Auckland, Auckland, New Zealand. He is currently working as a Professor with the School of Electrical and Power Engineering, China University of Mining and Technology, Xuzhou, China. His research interests include wireless power transfer and intelligent control.

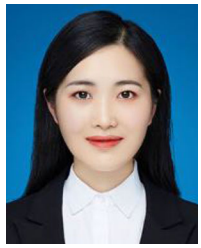

Nan Wei received the B.S. degree in electrical engineering from Yancheng Institute of Technology, Yancheng, China, in 2019. She is currently working toward the M.S. degree with the School of Electrical and Power Engineering, China University of Mining and Technology, Xuzhou, China.

Her research interests include wireless power transfer.

Hongtai Zhang received the B.S. degree in electrical engineering in 2018 from China University of Mining and Technology, Xuzhou, China, where he is currently working toward the M.S. degree with the School of Electrical and Power Engineering.

His research interests include wireless power transfer.

Shuze Zhao received the B.S. degree in electrical engineering in 2018 from China University of Mining and Technology, Xuzhou, China, where he is currently working toward the M.S. degree with the School of Electrical and Power Engineering.

His research interests include wireless power transfer.

Zhuang Li received the B.S. degree in electrical engineering in 2019 from China University of Mining and Technology, Xuzhou, China, where he is currently working toward the M.S. degree with the School of Electrical and Power Engineering.

His research interests include wireless power transfer.

Zhijuan Liao received the B.E. and Ph.D. degrees from the College of Automation, Chongqing University, Chongqing, China, in 2014 and 2019, respectively.

She is currently working as a Lecturer with the School of Electrical and Power Engineering, China University of Mining and Technology, Xuzhou, China. Her research interests include wireless power transfer and power electronics.